Estimation of oceanic sub-surface mixing under a severe cyclonic storm using a coupled atmosphere-ocean-wave model

Kumar Ravi Prakash, Tanuja Nigam, Vimlesh Pant

Centre for Atmospheric Sciences, Indian Institute of Technology Delhi, New Delhi-110016

Abstract

A coupled atmosphere-ocean-wave model used to examine mixing in the upper oceanic layers under the influence of a very severe cyclonic storm Phailin over the Bay of Bengal (BoB) during 10-14 October 2013. Model simulations highlight prominent role of cyclone induced near-inertial oscillations in sub-surface mixing up to the thermocline depth. The inertial mixing introduced by the cyclone played a central role in deepening of the thermocline and mixed layer depth by 40 m and 15 m, respectively. A detailed analysis of inertial oscillation kinetic energy generation, propagation, and dissipation was carried out at a location in northwestern BoB. ~~The peak magnitude of kinetic energy in baroclinic and barotropic currents found to be 1.2 $m^2 s^{-2}$ and 0.3×10^{-2} $m^2 s^{-2}$, respectively. The power spectrum analysis suggested a dominant frequency operative in sub-surface mixing was associated with near-inertial oscillations. The peak strength of 0.84 $m^2 s^{-1}$ in zonal baroclinic current found at 14 m depth. The baroclinic kinetic energy remain higher (> 0.03 $m^2 s^{-2}$) during 11-12 October and decreased rapidly thereafter. The wave number rotary spectra identified the downward propagation, from surface up to the thermocline, of energy generated by inertial oscillations. A quantitative analysis of shear generated by the near-inertial baroclinic current showed higher shear generation at 40-80 m depth during peak surface winds. Analysis highlights that greater mixing within the mixed layer take place where the eddy kinetic diffusivity was high (> 6×10^{-11} $m^2 s^{-1}$). The turbulent kinetic energy dissipation rate increased from 4×10^{-14} to 2.5×10^{-13} W kg^{-1} on approaching the thermocline that dampened mixing process further downward into the thermocline layer.~~ Large shear generated by the inertial oscillations found to overcome the stratification and initiate mixing at the base of the mixed layer. Greater mixing was found at the depths where the eddy kinetic diffusivity was large. The baroclinic current, holding a larger fraction of kinetic energy than the barotropic current, weakened rapidly after the passage of cyclone. The shear-induced by inertial oscillations found to decrease rapidly with increasing depth below the thermocline. The dampening of mixing process below the thermocline explained

through the enhanced dissipation rate of turbulent kinetic energy upon approaching the thermocline layer. The wave-current interaction, non-linear wave-wave interaction were found to affect the process of downward mixing and cause the dissipation of inertial oscillations.

1. Introduction

The Bay of Bengal (BoB), a semi-enclosed basin in the northeastern Indian ~~Ocean~~ocean, consists of surplus near-surface fresh water due to large precipitation and runoff from the major river systems of the Indian subcontinent (Varkey et al., 1996; Rao and Sivakumar, 2003; Pant et al., 2015). Presence of fresh water leads to salt-stratified upper ocean water column and formation of barrier layer (BL), a layer sandwiched between bottom of the mixed layer (ML) and top of the thermocline, in the BoB (Lukas and Lindstrom, 1991; Vinayachandran et al., 2002; Thadathil et al., 2007). The BL restricts entrainment of colder waters from thermocline region into the mixed layer thereby, maintains warmer ML and sea surface temperature (SST). The warmer SST together with higher tropical cyclone heat potential (TCHP) makes the BoB as one of the active regions for cyclogenesis (Suzana et al. 2007; Yanase et al. 2012, Vissa et al. 2013). Majority of tropical cyclones generate during the pre-monsoon (April-May) and post-monsoon (October-November) seasons (Alam et al., 2003; Longshore, 2008). The number of cyclones and their intensity is highly variable in seasonal and interannual time scales. The stratification of the ~~Ocean~~ ocean is one of the important factors to drive the ocean response of the tropical cyclone. The BL formation in the BoB is associated with the strong stratification due to the peak discharge from rivers in the post-monsoon season. The intensity of the cyclone largely depends on the degree of stratification (Neetu et al. 2012; Li et al. 2013).

Mixing in the water column has an important role in energy and material transference. Mixing in the ocean can be introduced by the different agents such as wind, current, tide, eddy, and cyclone. Mixing due to tropical cyclones is mostly limited to the upper ocean but the cyclone-induced internal waves can affect the subsurface mixing. Several studies have observed that the mixing in the upper oceanic layer is introduced due to the generation of near-~~-~~inertial oscillations (NIO) during the passage of tropical cyclones (Gonella, 1971; Shay et al., 1989; Johanston et al., 2016). This mixing is responsible for deepening of ML and shoaling of the thermocline (Gill, 1984). The vertical mixing caused by storm-~~–~~induced NIO has a significant impact on the upper ocean variability (Price, 1981). The NIO are also found to be responsible for the decrement of SST along the cyclone track (Chang and Anthes, 1979; Leipper, 1967; Shay et al., 1992; Shay et al., 2000). This decrease in SST is caused by the entrainment of cool subsurface thermocline water in the mixed layer into the immediate overlying layer of water. This cooling of surface water is one of the components of the decaying mechanism of the stormy event (Cione and Uhlhorn, 2003). There is a remarkable difference in the magnitude of this cooling of surface temperature moving on the highly stratified to less or weakly stratified bay locations those are falling at the rightward to the cyclone track (Jacob, 2003; Price et al., 1981).

The near-~~–~~inertial process can be analyzed from the baroclinic component of currents. The vertical shear of horizontal baroclinic velocities that is interrelated to buoyancy oscillations of surface layers ~~are~~ is utilized in various studies to have an adequate understanding of the mixing associated with high frequency oscillations i.e. NIO (Zhang et al., 2014). The shear generated due to NIO is an ~~one of the~~ important factor ~~other than the wind stress~~ for the intrusion of the cold thermocline water into the ML during near-~~–~~inertial scale mixing (Price et al., 1978; Shearman, 2005; Burchard and Rippeth, 2009). The alternative upwelling and downwelling features of the temperature profile are an indication of the inertial mixing. The Kinetic energy bounded with these components of current shows a rise in magnitude at the right side of cyclone track (Price et al., 1981; Sanfoard et al., 1987; Jacob, 2003). The reason for this high magnitude of kinetic energy is linked with strong wind and rotating wind vector condition of the storm.

In several studies (Chang et al., 2008; Lin et al., 2008; Shang et al., 2008; Lin et al., 2003; Zhao et al., 2009), upper ~~Ocean~~ ocean response for various cyclonic events is also inspected and proved for the enhancement of primary productivity during post-~~–~~cyclone state of the ~~Ocean~~ ocean. At the time when a storm is active and prior to it, the surface concentration of chlorophyll-a (Chl-a), a proxy for the concentration of primary productivity is comparatively lower than that of the post-cyclonic state of the ocean surface (Sarangi, 2011, Latha et al., 2015). This increment in the chlorophyll is dependent on the relative entrainment of the cool subsurface water, enriched in nutrient under the influence of energetic near-~~–~~inertial wave mixing caused by the tropical cyclones.

The ~~Aim~~aim of this paper is to understand and quantify the near-~~-~~inertial mixing due to the Phailin, a very severe cyclonic storm (VSCS) in the BoB. The study also focuses on analyzing the subsurface distribution of NIO with its vertical mixing potential. Further, the study quantifies the shear generated mixing and the kinetic energy of the~~se~~ baroclinic mode of horizontal current varying in the vertical section at a selected location during the active period of the cyclone. The dissipation rate of NIO and turbulent eddy diffusivity are quantified.

2. Data and Methodology

2.1 Model details

Numerical simulations during the period of VSCS Phailin were carried out using the coupled ~~Ocean-Atmosphere-wave-Sediment~~ ocean-atmosphere-wave-sediment transport (COAWST), described in detail by Warner et al. (2010). COAWST modeling system couples the three-dimensional oceanic model 'Regional Ocean Modeling System' (ROMS), the atmospheric model 'Weather Research and Forecasting' (WRF), and the wind wave generation and propagation model 'Simulating Waves Nearshore' (SWAN). ROMS model used for the study is a free surface, primitive equation, sigma coordinate model. ROMS is a hydrostatic ocean model that solves finite difference approximations of the Reynolds averaged Navier-S~~s~~tokes equations (~~c~~Chassignet et al 2000; Haidvogel et al. 2000, Haidvogel et al. 2008; Shchepetkin and McWilliams 2005). The atmospheric model component in the COAWST is a non-hydrostatic, compressible model 'Advanced Research Weather Research Forecast Model' (WRF-ARW), described in Skamarock et al., (2005). It has different schemes for representation of boundary layer physics and physical parameterizations of sub-grid scale processes. In the COAWST modeling system, appropriate modifications were made in the code of atmospheric model component to provide an improved bottom roughness from the calculation of the bottom stress over the ocean (Warner et al., 2010). Further, the momentum equation is modified to improve the representation of surface waves. The modified equation needs the additional information of wave energy dissipation, propagation direction, wave height, wave~~-~~length that are obtained from wave component of the COAWST model.

The spectral wave model SWAN, used in the COAWST modeling system, is designed for shallow water. The wave action balance equation is solved in the wave model for both spatial and spectral spaces (Booij et al. 1999). ~~In the COAWST, the ocean model ROMS simulated free surface~~

~~elevations (ELV), and current (CUR) are provided to the wave model SWAN. The Kirby and Chen (1998) formulation has been used for the computation of current. The Model Coupling Toolkit (MCT) used as a coupler in the COAWST modeling system to couple different model components (Larson et al., 2004; Jacob et al., 2005). A parallel-coupled approach is utilized by the coupler that permits the transmission and transformation of various distributed parameters between component models. MCT coupler facilitates exchanges of prognostic variables from one model to another model components. Further details on various parameters exchanged among the component models of COAWST modeling system can be found in Warner et al. (2010).~~The SWAN model used in the COAWST system includes the wave-wind generation, wave-breaking, wave-dissipation, and nonlinear wave-current-wind interaction. The 'Model Coupling Toolkit' (MCT) used as a coupler in the COAWST modeling system to couple different model components (Larson et al., 2004; Jacob et al., 2005). The coupler utilizes a parallel-coupled approach to facilitate the transmission and transformation of various distributed parameters among component models. MCT coupler exchanges prognostic variables from one model to another model component as shown in Figure 1. The WRF model receives sea surface temperature (SST) from the ROMS model and supplies the zonal (Uwind) and meridional (Vwind) components of 10-m wind, atmospheric pressure (Patm), relative humidity (RH), cloud fraction (Cloud), precipitation (Rain), shortwave (Swrad) and longwave (Lwrad) radiation to the ROMS model. The SWAN model receives Uwind and Vwind from the WRF model and transfers significant wave height (Hwave) and mean wavelength (Lmwave) to the WRF model. A large number of variables are exchanged between ROMS and SWAN models. The ocean surface current components (Us, Vs), free surface elevations (η), and bathymetry (Bath) provided to the SWAN from ROMS model. The wave parameters i.e. Hwave, Lmwave, peak wavelength (Lpwave), wave direction (Dwave), surface wave period (Tpsurf), bottom wave period (Tmbott), percentage wave breaking (Qb), wave energy dissipation (DISSwcap), and bottom orbit velocity (Ubot) provided from the SWAN to ROMS model through the MCT coupler. Further details on the COAWST modeling system can be found in Warner et al. (2010).

Formatted: Indent: First line: 1.27 cm

2.2 Model configuration and experiment design

The coupled model was configured over the BoB to study the VSCS Phailin during the period of 10 to 15 October 2013. The setup of COAWST modeling system used in this study included fully coupled atmosphere-ocean-wave (ROMS+WRF+SWAN) models but the sediment transport is not included. A non-hydrostatic, fully compressible atmospheric model with a terrain-following vertical coordinate system, WRF-ARW (version 3.7.1) was used in the COAWST configuration. The WRF model used with 9 km horizontal grid resolution over the domain 65 °E-105 °E, 1°N-34 °N and 30 sigma levels in the vertical. WRF was initialized with ‘National Centre for Environmental Prediction’ (NCEP) ‘Final Analysis’ (FNL) data (NCEPFNL, 2000) at 00 GMT on 10th October 2013. The lateral boundary conditions in WRF were provided at 6 hour interval from the FNL data. ~~The atmospheric model~~ We used the parameterization schemes for calculating boundary layer processes, precipitation processes, and surface radiation fluxes. The Monin-Obukhov scheme of surface roughness layer parameterization (Monin and Obukhov 1954) was activated in the model. The Rapid Radiation Transfer Model (RRTM) and cloud-interactive shortwave (SW) radiation scheme from Dudhia (1989) were used. The planetary boundary layer scheme YSU-PBL, described by Noh et al. (2003), was used. At each time step, the calculated value of exchange coefficients and surface fluxes off the land or ocean surface by the atmospheric and land surface layer models (NOAH) passed to the YSU PBL. The Grid-scale precipitation processes were represented by WRF single-moment (WSM) six-class moisture microphysics scheme by Hong and Lim (2006). The sub-grid scale convection and cloud detrainment were taken care by Kain (2004) cumulus scheme.

A terrain following ocean model ROMS with 40 sigma levels in the vertical used in this study. The ROMS model domain used with zonal and meridional grid resolutions of 6 km and 4 km, respectively. This high resolution in ROMS enables to resolve mesoscale eddies in the ocean. The vertical starching parameters i.e. θ_s and θ_b were set at 7 and 2, respectively. The northern lateral boundary in ROMS was closed by the Indian subcontinent. The ROMS model observed open lateral boundaries in the west, east, and south in the present configuration. The initial and lateral open boundary conditions were derived from the ‘Estimating the Circulation and Climate of the Ocean, Phase II’ (ECCO2) data. The ocean bathymetry was provided from the 2-minute gridded global relief data (ETOPO2). There was no relaxation provided to the model for any correction in the temperature, salinity, and current fields. ~~A terrain following ocean model ROMS with 40 sigma levels used in this study.~~ The Generic-Length-Scale (GLS) vertical mixing scheme parameterized as the K-ε model used (Warner et al., 2005). Tidal boundary conditions were derived from the TPXO.7.2 (ftp://ftp.oce.orst.edu/dist/tides/Global) data, which includes phase and amplitude of the M2, S2, N2, K2, K1, O1, P1, MF, MM, M4, MS4, and MN4 tidal constituents along the east coast of India. The tidal input was interpolated from

Formatted: Subscript

Formatted: Subscript

TPXO.7.2 grid to ROMS computational grid. The Shchepetkin boundary condition (Shchepetkin, 2005) for the barotropic current was used at open lateral boundaries of the domain which allowed the free propagation of astronomical tide and wind-~~-~~generated currents. The domains of atmosphere and ocean models which were part of the COAWST modeling system are shown in Figure 2~~1~~. ~~The domain for SWAN model was similar to the domain of ROMS model~~The ROMS and SWAN were configured over the common model domain. The WAVE model (SWAN) was forced with the WRF computed wind field. We used 24 frequency (0.04 - 1.0 Hz) and 36 directional bands. The boundary conditions for SWAN was derived from the 'WaveWatch III' model. ~~The atmospheric model WRF had 9 km horizontal grid resolution over the domain 65 °E-105 °E, 1°N-34 °N with 30 sigma levels in vertical. WRF was initialized with National Centre for Environmental Prediction (NCEP) Final Analysis (FNL) data (NCEP-FNL, 2000) on 10th October 2013 at 00 GMT. Lateral boundary conditions in WRF provided at 6 h interval from the FNL data. The ROMS model domain had zonal and meridional grid resolutions of 6 km and 4 km, respectively. The northern lateral boundary in ROMS was closed and the model observed open boundaries in rest of the sides. The oceanic initial and lateral open boundary conditions were derived from the Estimating the Circulation and Climate of the Ocean, Phase II (ECCO2) data. Ocean bathymetry was derived from 2-minute gridded global relief data (ETOPO2).~~ In the COAWST system, the free surface elevations (ELV) and current (CUR) simulated by ocean model ROMS are provided to the wave model SWAN. The Kirby and Chen (1998) formulation has been used for the computation of current. The surface wind applied to the SWAN model (provided by WRF) used in the Komen et al. (1984) closure model to transfer energy from the wind to wave field. The baroclinic time step used in ROMS model was 5 s. The SWAN and WRF models used with time steps of 120 s and 60 s, respectively. The coupled modeling system allows the exchange of prognostic variables among the atmosphere, ocean, and wave models at every 600 s. The SST simulation at high spatial and temporal resolutions enables accurate heat fluxes at the air-sea interface and exchange of heat between oceanic mixed layer and atmospheric boundary layer. The surface roughness parameter calculated in the WRF model based on Taylor and Yelland (2001), which involved parameters from the wave model. ~~The Advanced Very High Resolution Radiometer (AVHRR) data was used for the validation of model simulated SST.~~

2.3. Methodology

The baroclinic current component was calculated by subtracting the barotropic component from the mean current with a resolution of 2 m in the vertical. The power spectrum analysis was performed on the zonal and meridional baroclinic currents along the depth section of the selected location by using periodogram method. The continuous wavelet transform using Morlet wavelet method carried out to analyze the temporal variability of the baroclinic current at a particular level of 14 m. The near-inertial baroclinic velocities were filtered by the Butterworth 2nd order scheme for the cutoff frequency range of 0.033 to 0.043. The filtered zonal (u_f) and meridional (v_f) inertial baroclinic currents were used to calculate the inertial baroclinic kinetic energy (E_f) in m^2 s^{-2} and inertial shear (S_f) following Zhang et al. (2014) using equation (1).

$$S_f = \left(\frac{\partial u_f}{\partial z}\right)^2 + \left(\frac{\partial v_f}{\partial z}\right)^2 \qquad (1)$$

As the stratification is a measure of oceanic stability, the buoyancy frequency (N) was calculated using equation (2)

$$N^2 = -\frac{g}{\rho}\frac{\partial \rho}{\partial z} \qquad (2)$$

Where ρ is the density of sea-water and g is acceleration due to gravity.

The analysis of generation of the inertial oscillations and their dissipation was performed on the basis of turbulent dissipation rate (ϵ) and turbulent eddy diffusivity (k_ρ).These parameters were calculated by using following formula (Mackinnon and Gregg, 2005; van der Lee and Umlauf, 2011; Palmer et al., 2008; Osborn, 1980)

$$\varepsilon = \varepsilon_0 \left(\frac{N}{N_0}\right)\left(\frac{S_{lf}}{S_0}\right) \qquad (3)$$

$$k_\rho = 0.2\, x \left(\frac{\varepsilon}{N^2}\right) \qquad (4)$$

Where S_{lf} is the low shear background velocity, Values of $N_0 = S_0 = 3$ cycle per hour and $\varepsilon_0 = 10^{-8}$ W kg^{-1}.

3. Results and Discussion

3.1. Details of VSCS Phailin

Phailin, a very severe cyclonic storm (VSCS) was developed over the BoB in the northern Indian ~~Ocean~~ ocean in October 2013. The landfall of Phailin occurred on 12 October 2013 around 15:30 GMT near Gopalpur district of Odisha state ~~at~~ on the east coast of India. After the 1999 super cyclonic event of the Odisha coast, Phailin was the second strongest cyclonic event that made ~~landfall at~~landfall on the east coast of India (Kumar and Nair, 2015). The low-~~-~~pressure system developed in the north of the Andaman Sea on 7^{th} October 2013, which transformed into a depression on 8^{th} October at 12 °N, 96 °E. This depression got converted to a cyclonic disturbance on 9^{th} October and further intensified while moved to east-central BoB and opted the maximum wind speed of 200 km h^{-1} at 03:00 GMT on 11^{th} October. Finally, landfall occurs at 17:00 GMT 12^{th} October. More details on the development and propagation of VSCS Phailin can be found in the literature (IMD Report, 2013; Mandal et al. 2015; Prakash and Pant, 2017).

3.2 Validation of coupled model simulations

The WRF model simulated track of Phailin was validated against the India Meteorological Department (IMD) reported best-track of the cyclone. A comparison of model simulated track with the IMD track is shown in Figure 3~~2~~. Solid circles marked on both the tracks represent the 6-hourly positions of the cyclone's center, as identified by the minimum surface pressure. WRF model in the coupled configuration does a fairly good job in simulating the track, translational speed, and landfall location of Phailin. The positional track error was about 40 km when compared to IMD track of Phailin. The ROMS model simulated SST ~~was~~ validated against the Advanced Very High Resolution Radiometer (AVHRR) satellite data on each day for the period of Phailin passage over the BoB. Figure 4~~3~~ shows that the coupled model simulations are capturing the SST features as well as the magnitude of cooling associated with the storm. The maximum cooling of the sea surface observed on 13^{th} October in the northwestern BoB in both, model and observations. This post-cyclone cooling primarily associated with the cyclone-induced upwelling resulting from the surface divergence driven by the Ekman transport. Thus, the coupled model is reproducing dynamical processes and vertical velocities reasonably well.

3.3. Cyclone induced mixing

The coupled atmosphere-ocean-wave simulation is an ideal tool to understand air-sea exchange of fluxes and their effects on the oceanic water column. Surface wind sets up currents on the surface as well as initiate mixing in the interior of the upper ocean. In order to examine the strength of mixing due to VSCS Phailin, the model simulated vertical temperature profile together with the zonal and meridional components of ~~wind~~current at a location 18.75 °N, 86.66 °E are plotted in Figure 5~~4~~. The ~~T~~temperature of the upper surface water (25 m -30 m) decreased by 3.5°C from its maximum value of 28 °C after the landfall of the cyclone on 12-13th October (Figure 5~~4~~a). In response to the strong cyclonic winds, the depth of 23 °C isotherm (D23) deepening from 50 m to 90 m was observed during 04-12 GMT on 12 October. At the same time, the mixed layer depth (MLD), denoted by a thick black line in Figure 5a, deepens by about 15 m. Based on the density criteria, we calculated MLD as the depth where density increased by 0.125 kg m^{-3} from its surface value. The inertial mixing introduced by the cyclone play central role in deepening of D23 and MLD on 12th October 2013. The warmer near-surface waters mixed downward when the cyclone crossed over this location. After the passage of cyclone, shoaling of D23 and MLD observed as a consequence of cyclone induced upwelling that entrain colder waters from the thermocline into the mixed layer. To examine the role of cyclone induced mixing in modulating the thermohaline structure of upper ocean, we carried out further analysis on the coupled model simulations as discussed in the following sections.

Formatted: Superscript

3.3.1. Kinetic energy distribution

During the initial phase of VSCS Phailin, the zonal and meridional currents were primarily westward and southward, respectively (Figures ~~4~~5b, ~~4~~5c). However, on and after 12th October when cyclone attains peak intensity and crosses over the location, alternative temporal sequences of westward/eastward~~ movement~~ in zonal current and southward/northward~~ flow~~ in meridional current were noticed in current profiles (Figures ~~4~~5b, ~~4~~5c). The ~~F~~frequency of these reversals in zonal and meridional currents are recognized as near-inertial frequency generated from the storm at this location (18.75 °N, 86.66 °E). The direction and magnitude of currents represent a variability within 16-24 hr that corresponds to the near-inertial time period for the selected location. Kinetic energy (KE) of currents at various depths is a proxy of energy available in the water column that becomes conducive ~~for~~to turbulent and inertial mixing. Time series of KE associated with the barotropic and depth-~~-~~averaged baroclinic components of current at the point location (18.75° N, 86.66° E)~~ are~~ is illustrated in Figure ~~4~~5d. The KE associated with the baroclinic component found to be much higher than the barotropic component of current. The depth-averaged baroclinic and barotropic current components' KE also depict the impinging oscillatory behavior. The peak magnitude of KE in baroclinic and barotropic currents found to be 1.2 $m^2\ s^{-2}$ and 0.3×10^{-2} $m^2\ s^{-2}$, respectively on 12th October at 08:00 GMT. It is worth noting that the time of peak KE in baroclinic currents (Figure 5d) coincide with the deepening of MLD and D23 (Figure 5a). Therefore, the KE generated in NIO is responsible for sub-surface mixing that acts to deepen the mixed layer. The analysis suggests that energy available for mixing process in the water column was mostly confined ~~in~~to the baroclinic currents at various depths.

3.3.2. Primary frequency and depth of mixing

The power spectrum analysis was performed on the time series profiles at selected point location (18.75 °N, 86.66 °E) to get a distribution of all frequencies operating in the mixing process during the passage of cyclone. As found in the previous section, the KE associated with baroclinic currents are dominated over the barotropic currents, the power spectrum analysis performed on zonal and meridional components of the baroclinic current profile is shown in Figure ~~5~~6. It is clear from Figure ~~5~~6 that tidal (M2, the semidiurnal component of tide) and near-inertial oscillations (f) are two dominant frequencies on the surface during the cyclone Phailin.~~ Further, the near-inertial frequency is smaller than the tidal frequency on the surface.~~ To analyze the mixing potential of the NIO, power spectrum method was applied ~~at~~to the profile of baroclinic current component~~ (Figure 5)~~. The largest power of the NIO was noticed at 14 m depth but the tidal oscillations were absent along the whole vertical section of baroclinic current (Figure 6). This finding motivated us to analyze the significance and distribution of ~~these~~this sub-surface variability that resulted in~~to~~ an anomalous deepening of MLD. The ~~H~~highest power of this signal was associated within 0-15 m with the magnitude of 0.84 $m^2\ s^{-1}$ in zonal baroclinic current and within 0-38 m with the magnitude of 0.76 $m^2\ s^{-1}$. These signals, however, weaken with increasing depth and almost disappeared around 120 m depth. These NIO were ~~are~~ the strongest signals at the 14 m depth that ~~and dominating~~ dominated the mixing compared to any process other than local wind stress. ~~by any~~

~~other process than the local wind stress.~~Other processes include the background flows, the presence of eddies, variations in sea surface height, non-linear wave-wave and wave-current interactions (Guan et al., 2014; Park and Watts, 2005).

In order to analyze the time distribution of the strong NIO, wavelet transform analysis was applied on the zonal and meridional baroclinic currents at 14 m depth. The Scalogram, shown in Figure ~~6~~7, depicts the generation of NIO signal on 12^{th} October that subsequently got strengthen and attains its peak value on the mid of 13^{th} October. The energy percentage of the meridional component was always lower than the zonal component. The peak values of energy percentage was found in the time periods between 25-28 hr~~ marked with a white dashed line in Figure 6~~. A Butterworth 2^{nd} order band~~-~~pass filter was applied at the corresponding cutoff frequency interval of 0.033 - 0.043 to filter the NIO signal of the baroclinic zonal and meridional currents. Figure ~~7~~8 shows profiles of near-inertial zonal (U_f) and meridional (V_f) baroclinic currents together with the kinetic energy (E_f) of near-inertial flow. The maximum strength of inertial baroclinic current was 0.3 m s^{-1} with the signature of an alternate directional reversal of current signals. Presence of these inertial currents~~ were~~was up to 70 m depth with the peak value of kinetic energy E_f being 0.048 m^2 s^{-2}. Stronger (>0.5 m s^{-1}) zonal and meridional baroclinic currents were observed up to 40 m depth. It can be noticed from Figure ~~7~~8c, the baroclinic kinetic energy remains higher (> 0.03 m^2 s^{-2}) only from mid of 11^{th} October ~~till~~until the end of 12^{th} October and decreased rapidly thereafter. ~~the energy rapidly decreases and almost disappeared after 13th October.~~ This indicates the period of prominent mixing due to NIO was 11-12 October 2013. The baroclinic kinetic energy almost ceased after 13^{th} October. The daily averaged values of baroclinic kinetic energy (not shown here) also confirms the maxima in E_f on 11-12 October with the vertical extent up to 80 m depth.

3.3.3. Role of downward propagation of energy

To investigate the energy propagation from the surface to the interior layers of upper-ocean, we derived the rotary spectra of near-inertial wave numbers and shown in Figure ~~8~~9. The daily averaged vertical wave-number rotary spectra provides a clear picture of wind energy distribution in the sub-surface water. The anticyclonic spectrum (A_m) is dominating over the cyclonic spectra (C_m) for the entire duration of the cyclone. This feature indicates that the energy is propagating downward generated by these inertial oscillations. The ~~M~~magnitude of these oscillations increased from initial stage up to 12^{th} October and remained at high energy density for

Formatted: Superscript

Formatted: Superscript

Formatted: Subscript

Formatted: Subscript

the rest of the cyclone period. This downward directed energy initiated a process of mixing between the mixed layer and the thermocline. This energy helps to deepen the mixed layer against oceanic stratification by introducing a strong shear. The buoyancy of stratified ocean was overcome to some extent by the shear generated that assist in mixing process during the very severe cyclone. For the current case, kinetic energy (Figure ~~7~~8c) represents the analogical behavior as reported by Alford and Gregg (2001). Their study highlighted that, in most of the cases, the energy of inertial oscillations potentially penetrates the mixed layer but suddenly drops down as it touches the thermocline. The energy dissipation mechanism studied in few other studies (Chant, 2001; Jacob, 2003).

The 2-layer model described by Burchard and Rippeth (2009) illustrated the process of generation of sufficient shear to start mixing near the thermocline. Their simple model ignored the effect of the lateral density gradient, mixing, and advection. Burchard et al. (2009) mentioned four important parameters for the shear generation, i.e. surface wind stress ($P_S S^2$), bed stress ($-D_b S^2$), interfacial stress ($-D_I S^2$), and barotropic flow ($P_m S^2$). Utilizing simulations from our coupled atmosphere-ocean-wave model, we calculated individual terms as suggested by Burchard et al. (2009) and presented in Figure ~~9~~10. ~~It is clear from the figure that the surface wind stress term plays most significant role~~ Surface wind stress found to be the most dominating term in modulating the magnitude of bulk shear during the stormy event. Rest of the terms were ~~Other terms were found to be~~ relatively weaker and, therefore, contributing only marginally ~~in~~ to the variability of the bulk shear.

To examine the generation and dissipation of these inertial waves, the shear generated by the near-inertial baroclinic current (S_f^2) and turbulent kinetic energy dissipation rate (ε) were calculated and analyzed. The shear produced by inertial oscillations ~~was increasing~~ increased at 20-80 m depth ~~from 40-80 m depth~~ and higher magnitude was associated with peak wind speed of cyclone (Figure ~~10a~~11a). This shear overcome the stratification (Figure ~~10b~~11b), represented by buoyancy frequency N^2~~-~~, and played important role in mixing and deepening of the thermocline and mixed layer on 12th October. ~~that was weak at this depth compared to the shear of the near-inertial waves.~~ The value of kinetic energy dissipation rate (ε) increased from 4×10^{-14} to 2.5×10^{-13} W kg^{-1} on approaching the thermocline (Figure ~~10c~~11c). The increase in ε indicates the weakening of the shear generated by the inertial waves leading to the fast disappearance of these

Formatted: Superscript

Formatted: Superscript

baroclinic instabilities from the region. The non-linear interaction between the NIO and internal tides together with the prevailing background currents cause rapid dissipation of kinetic energy in the thermocline. Guan et al. (2014) also reported an accelerated dampening of NIO associated with the wave-wave interactions between NIO and internal tides. The background currents found to modify the propagation of NIO (Park and Watts, 2005). The magnitude of the turbulent eddy diffusivity (K_ρ), shown in Figure ~~10d~~11d, implies that the greater mixing takes place within the mixed layer ~~place~~ where K_ρ was high (6.3×10^{-11} to 1.2×10^{-11} $m^2 s^{-1}$). The daily averaged values of ε and K_ρ were 1.2×10^{-13} W kg^{-1} and 1.5×10^{-10} $m^2 s^{-1}$, respectively on 12th October, which were higher as compared to the initial two days of the cyclonic event. ~~Therefore, r~~Results from the present study, as well as the conclusions from the past studies, indicate that wave-current interaction, mesoscale processes, and wave-wave interaction can affect the process of downward mixing and cause the dissipation of inertial oscillations.

4. Conclusions

Processes controlling the sub-surface mixing were evaluated under the high wind speed regime of a severe cyclonic storm Phailin over the BoB. A coupled atmosphere-ocean-wave (WRF+ROMS+SWAN) model as part of the COAWST modeling system was used to simulate atmospheric and oceanic conditions during the passage of Phailin cyclone. A detailed analysis of model simulated data revealed interesting features of generation, propagation, and dissipation of kinetic energy in the upper oceanic water column. Deepening of the MLD and thermocline by 15 m and 40 m, respectively were explained through the strong shear generated by the inertial oscillations that helped to overcome the stratification and initiate mixing at the base of the mixed layer. However, there was a rapid dissipation of the shear with increasing depth below the thermocline. The peak magnitude of kinetic energy in baroclinic and barotropic currents found to be 1.2 $m^2 s^{-2}$ and 0.3×10^{-2} $m^2 s^{-2}$, respectively. The power spectrum analysis suggested a dominant frequency operative in sub-surface mixing that was associated with near-inertial oscillations. The peak strength of 0.84 $m^2 s^{-1}$ in the zonal baroclinic current found at 14 m depth at a location in northwestern BoB. The baroclinic kinetic energy remains higher (> 0.03 $m^2 s^{-2}$) during 11-12 October and decreased rapidly thereafter. The wave-number rotary spectra identified the downward propagation, from the surface up to the thermocline, of energy generated by inertial oscillations. A quantitative analysis of shear generated by the near-inertial baroclinic current showed higher shear generation at 20-80 m depth during peak surface winds. Analysis highlights that greater mixing within the mixed layer takes place where the eddy kinetic diffusivity was high ($> 6\times10^{-11}$ $m^2 s^{-1}$). The turbulent kinetic energy dissipation rate increased from 4×10^{-14} to 2.5×10^{-13} W kg^{-1} on approaching the thermocline that dampened mixing process further down into the thermocline layer. ~~Kinetic energy associated with baroclinic currents were about two order of magnitudes higher than in barotropic component. The peak strength of 0.84 m^2 s^{-1} in zonal baroclinic current was found at 14 m depth at a location in northwestern BoB.~~ The wave-current interaction, mesoscale processes, and wave-wave interaction increased the dissipation rate of shear and, thereby, limited the downward mixing up to the thermocline. ~~were found to affect the process of downward mixing and cause the dissipation of inertial oscillations.~~ The coupled model found to be a useful tool to investigate air-sea interaction, kinetic energy propagation, and mixing in the upper ocean ~~and oceanic sub-surface processes~~.

Author contribution: KRP and TN performed model simulations and analyzed data. VP prepared the manuscript with contributions from all co-authors.

Acknowledgements

ECCO2 is a contribution to the NASA Modeling, Analysis, and Prediction (MAP) program. The study benefitted from the funding support from Ministry of Earth Sciences, Govt. of India and Space Applications Centre, Indian Space Research Organisation. High Performance Computing (HPC) facility provided by IIT Delhi and Department of Science and Technology (DST), Govt. of India are thankfully acknowledged. Authors are thankful to Dr. Lingling Xie for his productive suggestions. Graphics generated in this manuscript using Ferret and NCL. TN and KRP acknowledge MoES and UGC-CSIR, respectively for their doctoral fellowship support.

References

Alam, M. M., Hossain, M.A. and Shafee, S.: Frequency of Bay of Bengal cyclonic storms and depressions crossing different coastal zones, Int. J. Climatol., 23, 1119–1125, doi:10.1002/joc.927, 2003.

Alford, M.H., Gregg, M.C.: Near-inertial mixing: modulation of shear, strain and microstructure at low latitude. J. Geophys. Res. 106 (C8), 16947–16968, 2001.

Booij, N., Ris, R. C., and Holthuijsen, L. H.: A third-generation wave model for coastal regions, Part I, Model description and validation, J. Geophys. Res., 104(C4), 7649–7666, doi:10.1029/98JC02622, 1999.

Burchard, H., Rippeth, T.P.: Generation of bulk shear spikes in shallow stratified tidal seas. J. Phys. Oceanogr. 39, 969–985, 2009.

Chang, J., Chung, C.-C., Gong, G.-C.: Influences of cyclones on chlorophyll-a concentration and Synechococcus abundance in a subtropical western Pacific coastal ecosystem. Mar. Ecol. Prog. Ser. 140, 199–205, 2008.

Chang, S. W., and Anthes, F.A.: The mutual response of the tropical cyclone and the ocean. J. Phys. Oceanogr., 9, 128–135, 1979.

Chant, R.J.: Evolution of near-inertial waves during an upwelling event on the New Jersey Inner Shelf. J. Phys. Oceanogr. 31, 746–764, 2001.

Chassignet, E.P., Arango, H.G., Dietrich, D., Ezer, T., Ghil, M., Haidvogel, D.B., Ma, C.C., Mehra, A., Paiva, A.M., Sirkes, Z.: DAMEE-NAB: the base experiments. Dyn. Atmos. Oceans 32, 155–183, 2000.

Cione, J. J., and Uhlhorn, E.W.: Sea surface temperature variability in hurricanes: Implications with respect to intensity change, Mon. Weather Rev., 131, 1783–1796, doi:10.1175//2562.1, 2003.

Dudhia, J.: Numerical study of convection observed during the winter —monsoon experiment using a mesoscale two dimensional model. J Atmos Sci. 46, 3077–3107, 1989.

Gill, A. E.: On the behavior of internal waves in the wake of storms,J. Phys. Oceanogr., 14, 1129 – 1151, 1984.

Gonella, J.: A study of inertial oscillations in the upper layers of the oceans. Deep-Sea Res., 18, 775–788, 1971.

Guan, S., Zhao, W., Huthnance, J. Tian, J., and Wang, J.: Observed upper ocean response to typhoon Megi (2010) in the Northern South China Sea. J. Geophys. Res. Oceans, 119, 3134–3157, doi:10.1002/2013JC009661, 2014..

Haidvogel, D.B., Arango, H.G., Budgell, W.P., Cornuelle, B.D., Curchitser, E., Di Lorenzo, E., Fennel, K., Geyer, W.R., Hermann, A.J., Lanerolle, L., Levin, J., McWilliams, J.C., Miller, A.J., Moore, A.M., Powell, T.M., Shchepetkin, A.F., Sherwood, C.R., Signell, R.P., Warner, J.C., Wilkin, J.: Regional ocean forecasting in terrain-following coordinates: model formulation and skill assessment. Journal of Computational Physics 227, 3595–3624, -2008.

Haidvogel, D.B., Arango, H.G., Hedstrom, K., Beckmann, A., Malanotte-Rizzoli, P. Shchepetkin, A.F.: Model evaluation experiments in the North Atlantic Basin: Simulations in nonlinear terrain-following coordinates. Dyn Atmos Oceans 32, 239–281, 2000.

Hong, S.Y., Lim, J.O.J.: The WRF single-moment 6-class microphysics scheme (WSM6). J Korean Meteor Soc 42:2, 129-151, 2006.

IMD Report.: Very Severe Cyclonic Storm, PHAILIN over the Bay of Bengal (08-14 October 2013) A Report. India Meteorological Department, Technical Report, October 2013.

Jacob, S.D., Shay, L.K.: The role of oceanic mesoscale features on the tropical cyclone-induced mixed layer response: A case study. J. Phys. Oceanog., 33, 649- 676, 2003.

Jacob, R., Larson, J., Ong, E.: M x N Communication and Parallel Interpolation in CCSM Using the Model Coupling Toolkit. Preprint ANL/MCSP1225-0205. Mathematics and Computer Science Division, Argonne National Laboratory, 25 pp, 2005.

Johnston, T.M.S., Chaudhuri, D., Mathur, M., Rudnick, D.L., Sengupta, D., Simmons, H.L., Tandon, A., and Venkatesan, R.: Decay mechanisms of near-inertial mixed layer oscillations in the Bay of Bengal, Oceanography, 29(2): 180–191, doi:10.5670/oceanog.2016.50, 2016.

~~Kirby, J. T., and Chen T.M.: Surface waves on vertically sheared flows: Approximate dispersion relations, J. Geophys. Res., 94(C1),1013–1027, doi:10.1029/JC094iC01p01013, 1989.~~

Kain, J.S.: The Kain-Fritsch convective parameterization: An update. J Appl Meteor 43, 170–181, 2004.

Kirby, J. T., and Chen T.M.: Surface waves on vertically sheared flows~~:~~ Approximate dispersion relations.~~,~~ J. Geophys. Res., 94(C1),1013–1027, doi:10.1029/JC094iC01p01013, 1989. ~~1989.~~

Komen, G.J., Hasselmann, S., and Hasselmann, K.: On the existence of a fully developed wind-sea spectrum. J. Phys. Oceanogr., 14, 1271–1285. 1984.

Kumar VS, Nair A.M.: Inter-annual variations in wave spectral characteristics at a location off the central west coast of India. Ann Geophys 33:159–167, doi:10.5194/angeo-33-159, 2015.

Latha, T.P., Rao, K.H., Nagamani, P.V., Amminedu, E., Choudhury, S.B., Dutt, C.B.S., and Dadhwal, V.K.: Impact of Cyclone PHAILIN on chlorophyll-a concentration and productivity in the Bay of Bengal. International Journal of Geosciences 6:473–480, doi:10.4236/ijg.2015.65037, 2015.

Leipper, D. F.: Observed Ocean Conditions and Hurricane Hilda, 1964, J. Atmos. Sci., 24, 182–186, doi:10.1175/1520-0469(1967) 0242.0.CO;2, 1967.

Zhi, Li., Yu, W., Li, T., Murty, V.S.N., and Tangang, F.: Bimodal character of cyclone climatology in the Bay of Bengal modulated by monsoon seasonal cycle. J Climate 26:1033-1046. doi: 10.1175/JCLI-D-11-00627.1, 2013.

Lin, I.I., Liu, W.T., Wu, C.C., Wong, T.F., Hu, C., Chen, Z., Liang, W.D., Yang, Y., Liu, K.K.: New evidence for enhanced ocean primary production triggered by tropical cyclone. Geophys. Res. Lett. 30 (13), doi:10.1029/2003GL017141, 2003.

Lin, I.I., Wu, C.C., Pun, I.F., Ko, D.S.: Upper ocean thermal structure and the western North Pacific category-5 typhoons. Part I: ocean features and category-5 typhoon's intensification. Mon. Weather Rev. 136, 3288–3306, 2008.

Longshore, D.: Encyclopedia of Hurricanes, Typhoons, and Cyclones, 468 pp., Checkmark, New York, 2008.

Larson, J., Jacob, R., Ong, E.: The Model Coupling Toolkit: A New Fortran90 Toolkit for Building Multiphysics Parallel Coupled Models. Preprint ANL/MCS- P1208-1204. Mathematics and Computer Science Division, Argonne National Laboratory, 25 pp, 2004.

Lukas, R., and Lindstrom, E.: The mixed layer of the western equatorial Pacific Ocean, J. Geophys. Res., 96, 3343–3357, 1991.

~~MacKinnon, J.A., Gregg, M.C.: Mixing on the late-summer New England Shelf — solibores, shear and stratification. J. Phys. Oceanogr. 33 (7), 1476–1492, 2003.~~

MacKinnon, J.A., Gregg, M.C.: Spring Mixing: Turbulence and Internal Waves during Restratification on the New England Shelf. Journal of Physical Oceanography 35:12, 2425-2443 2005.

Mandal M., Singh K. S., Balaji M., Mohapatra M.: Performance of WRF-ARW model in real-time prediction of Bay of Bengal cyclone 'Phailin'. Pure Appl. Geophys DOI 10.1007/s00024-015-1206-7, 2015.

Monin, A.S., Obukhov, A.M.F.: Basic laws of turbulent mixing in the surface layer of the atmosphere. *Contrib Geophys Inst Acad Sci USSR 151:*163, e187, 1954.

National Centers for Environmental Prediction/National Weather Service/NOAA/U.S. Department of Commerce: NCEP FNL Operational Model Global Tropospheric Analyses, continuing from July 1999. Research Data Archive at the National Center for Atmospheric Research, Computational and Information Systems Laboratory. Dataset. https://doi.org/10.5065/D6M043C6, 2000.

Neetu, S., Lengaigne, M., Vincent, E.M., Vialard, J., Madec, G., Samson, G., Ramesh Kumar, M.R., and Durand, F.: Influence of upper-ocean stratification on tropical cyclone-induced surface cooling in the Bay of Bengal, J. Geophys. Res., 117, C12020, doi:10.1029/2012JC008433, 2012.

Noh, Y., Cheon, W.G., Hong, S.Y., Raasch, S.: Improvement of the K-profile model for the planetary boundary layer based on large eddy simulation data. Bound Layer Meteor 107, 401–427, 2003.

Osborn, T.R.: Estimates of the Local-Rate of Vertical Diffusion from Dissipation Measurements. J. Phys. Oceanogr. 10, 83–89, 1980.

Palmer, M.R., Rippeth, T.P., Simpson, J. H.: An investigation of internal mixing in a seasonally stratified shelf sea. J. Geophys. Res. 113, C12005, doi:10.1029/2007JC004531, 2008.

Pant V, Girishkumar M.S., Udaya Bhaskar T.V.S., Ravichandran M., Papa F., Thangaprakash V.P.: Observed interannual variability of near-surface salinity in the Bay of Bengal, J. Geophys. Res 120(5):3315–3329, 2015.

Park, J.H., and Watts, D. R.: Near-inertial oscillations interacting with mesoscale circulation in the southwestern Japan/East Sea. Geophys. Res. Lett., 32, L10611, doi: 10.1029/2005GL022936, 2005.

Prakash K.R., Vimlesh Pant: Upper oceanic response to tropical cyclone Phailin in the Bay of Bengal using a coupled atmosphere-ocean model, Ocean Dynamics, 67, 51-64, doi:10.1007/s10236-016-1020-5, 2017.

Price, J. F., Mooers, C.N., and Van Leer, J.C.: Observation and simulation of storm-induced mixed-layer deepening. J. Phys. Oceanogr., 8, 582-599, https://doi.org/10.1175/1520-0485(1978)008<0582:OASOSI>2.0.CO;2, 1978.

Price, J.F.: Upper ocean response to a hurricane. J. Phys. Oceanog., 11, 153-175, 1981.

Rao, R. R., and Sivakumar, R.: Seasonal variability of sea surface salinity and salt budget of the mixed layer of the north Indian Ocean, J. Geophys. Res., 108(C1), 3009, doi:10.1029/2001JC000907, 2003.

Sanford, T. B., Black, P.G., Haustein, J., Feeney, J.W., Forristall, G.Z., and Price, J.F.: Ocean response to a hurricane. Part I: Observations. J. Phys. Oceanogr., 17, 2065–2083, 1987.

Sarangi, R. K.: Remote-sensing-based estimation of surface nitrate and its variability in the southern peninsular Indian waters, Int. J. Oceanogr., doi:10.1155/2011/172731, 2011.

Shang, S., Li, L., Sun, F., Wu, J., Hu, C., Chen, D., Ning, X., Qiu, Y., Zhang, C., and Shang, S., Changes of temperature and bio-optical properties in the South China Sea in response to Typhoon Lingling, (2001), Geophys. Res. Lett., 35, L10602, doi:10.1029/2008GL033502, 2008.

Shchepetkinand A. F., McWilliams J. C.: The Regional Ocean Modeling System: A split-explicit, free-surface, topography following coordinates ocean model, *Ocean Modelling*, **9**, 347-404, 2005.

Skamarock, W.C., Klemp, J.B., Dudhia, J., Gill, D.O., Barker, D.M., Wang, W., Powers, J.G.: A Description of the Advanced Research WRF Version 2. NCAR Technical Note, NCAR/TN-468+STR., 2005.

Shay, L. K., Black, P., Mariano, A., Hawkins, J., and Elsberry, R.: Upper ocean response to hurricane Gilbert, J. Geophys. Res., 97(20), 227–248, 1992.

Shay, L. K. and Elsberry, R.L.: Vertical structure of the ocean current response to a hurricane. J. Phys. Oceanog., 19, 649-669, 1989.

Shay, L. K., Goni, G.J., and Black, P.G.: Effects of a warm oceanic feature on Hurricane Opal, Mon. Weather Rev., 128, 1366–1383, doi:10.1175/1520-0493(2000)1282.0.CO;2, 2000.

Shearman, R.K.: Observations of near-inertial current variability on the New England shelf. J. Geophys. Res. 110, C02012, doi:10.1029/2004JC002341, 2005.

Suzana, J Carmargo, Adam H Sobel, Anthony G Barnston and Kerry A. Emanuel: Tropical cyclone genesis potential index in climate models. Tellus 59A:428-443, 2007.

Taylor, P.K., and Yelland, M.J.: The dependence of sea surface roughness on the height and steepness of the waves. J. Phys. Oceanogr., 31, 572–590, 2001.

Thadathil, P., Muraleedharan, P.M., Rao, R.R., Somayajulu, Y.K., Reddy, G.V., and Revichandran, C.: Observed seasonal variability of barrier layer in the Bay of Bengal, J. Geophys. Res., 112, C02009, doi:10.1029/2006JC003651, 2007.

Varkey, M. J., Murty, V.S.N., and Suryanarayana, A.: Physical oceanography of the Bay of Bengal and Andaman Sea, Oceanogr. Mar. Biol., 34, 1–70, 1996.

van der Lee, E.M., and Umlauf, L.: Internal wave mixing in the Baltic Sea: near-inertial waves in the absence of tides. J. Geophys. Res. 116, C10016, doi:10.1029/2011JC007072, 2011.

Vinayachandran, P. N., Murty, V.S.N., and Ramesh Babu V.: Observations of barrier layer formation in the Bay of Bengal during summer monsoon, J. Geophys. Res., 107(C12), 8018, doi:10.1029/2001JC000831, 2002.

Vissa, N.K., Satyanarayana, A.N.V. and Prasad Kumar, B.: Intensity of tropical cyclones during pre- and post-monsoon seasons in relation to accumulated tropical cyclone heat potential over Bay of Bengal, Nat Hazards 68: 351. https://doi.org/10.1007/s11069-013-0625-y. 2013.

Warner, J. C., Sherwood, C.R., Arango, H.G., and Signell, R.P.: Performance of four turbulence closure models implemented using a generic length scale method, Ocean Modell., 8, 81–113, doi:10.1016/j. ocemod.2003.12.003, 2005.

Warner, J.C., Armstrong B., He R., Zambon J.B.: Development of a coupled ocean–atmosphere–wave–sediment transport (COAWST) modeling system. Ocean modelling 35:230–244. doi:10.1016/j. oceanmod.2010.07.010, 2010.

Yanase, W., Satosh, M., Taniguchi, H., and Fujinami, H.: Seasonal and Intraseasonal Modulation of tropical cyclogenesis environment over the Bay of Bengal during the extended summer monsoon. J Climate 25:2914-2930. doi: 10.1175/JCLI-D-11-00208.1, 2012.

Zhang, S., Xie, L., Hou, Y., Zhao, H., Qi, Y., & Yi, X.: Tropical storm-induced turbulent mixing and chlorophyll-a enhancement in the continental shelf southeast of Hainan Island. *Journal of Marine Systems*, *129*, 405-414, 2014.

Zhao, H., Tang, D.L., Wang, D.X.: Phytoplankton blooms near the Pearl River Estuary induced by Typhoon Nuri. J. Geophys. Res. 114, C12027, doi:10.1029/ 2009JC005384, 2009.

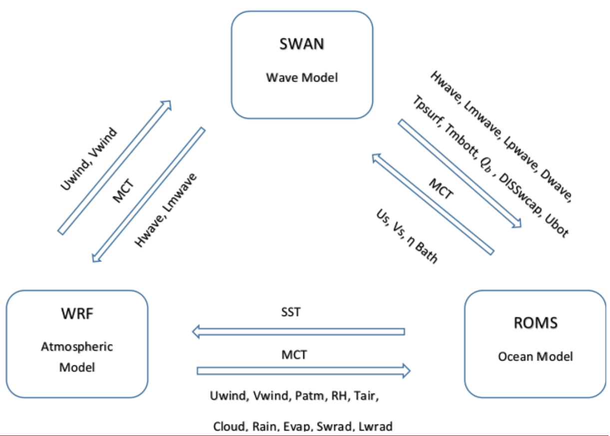

Figure 1:-The block diagram showing the component models WRF, ROMS, and SWAN of the COAWST modeling system together with the variables exchanged among the models. MCT- the model coupling toolkit is a model coupler used in the COAWST system.

Formatted: Justified

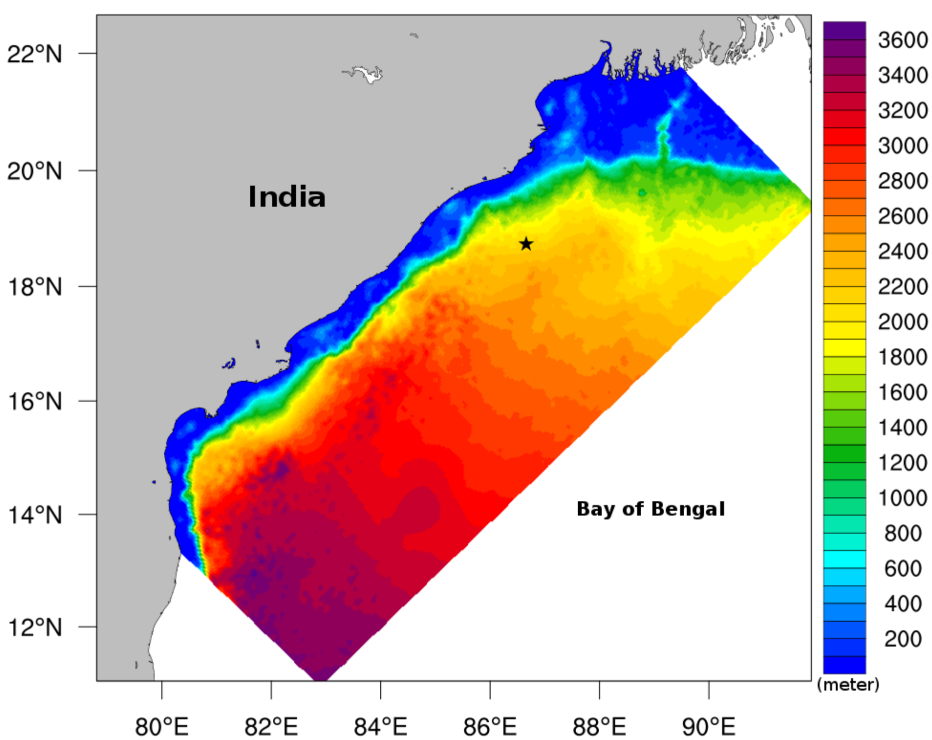
India
Bay of Bengal
22°N
20°N
18°N
16°N
14°N
12°N
80°E
82°E
84°E
86°E
88°E
90°E
3600
3400
3200
3000
2800
2600
2400
2200
2000
1800
1600
1400
1200
1000
800
600
400
200
(meter)

Figure 2~~1~~:-COAWST model domain (65°-105 °E, 1°-34 °N) overlaid with GEBCO bathymetry (m). Location used for time-series analysis marked with a star.

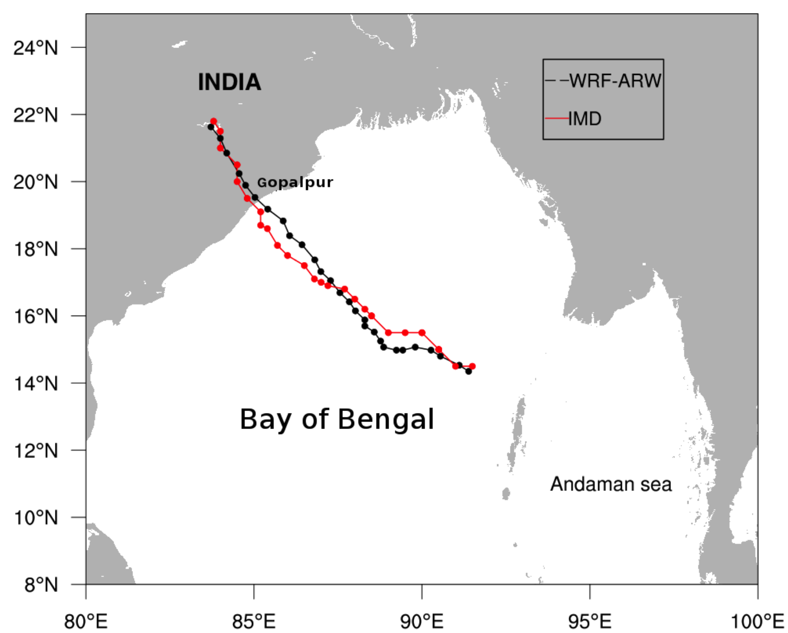

Figure 3~~2~~:- Validation of VSCS Phailin track simulated by coupled model (black) with IMD reported track (red).

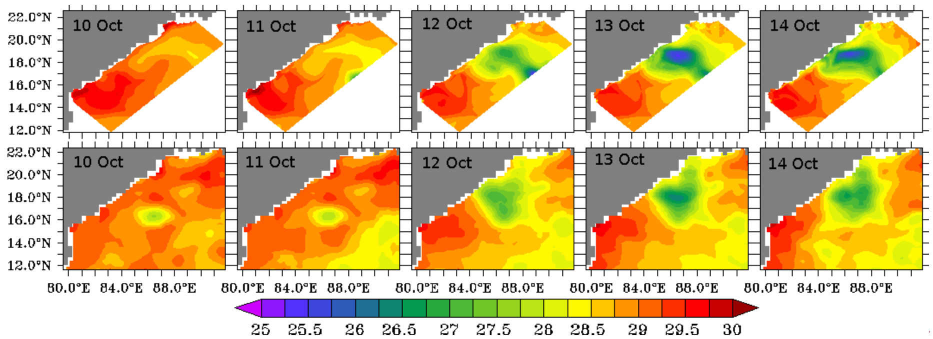

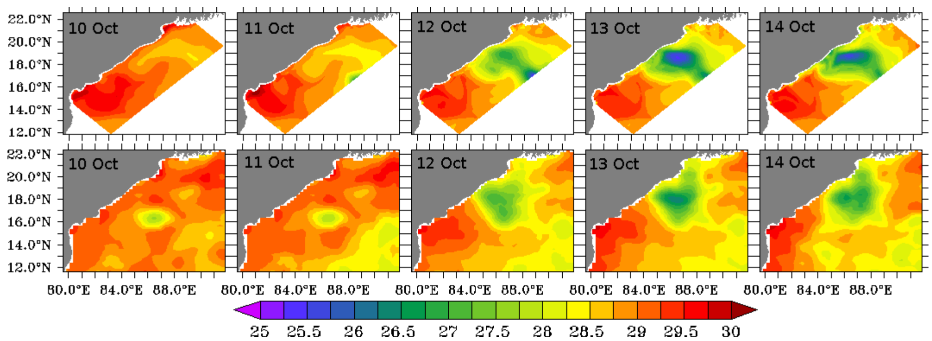

Figure 4~~3~~:- Sea ~~S~~surface ~~T~~temperature (SST) in °C observed from AVHRR sensor on the satellite (lower panel) and simulated by model (upper panel).

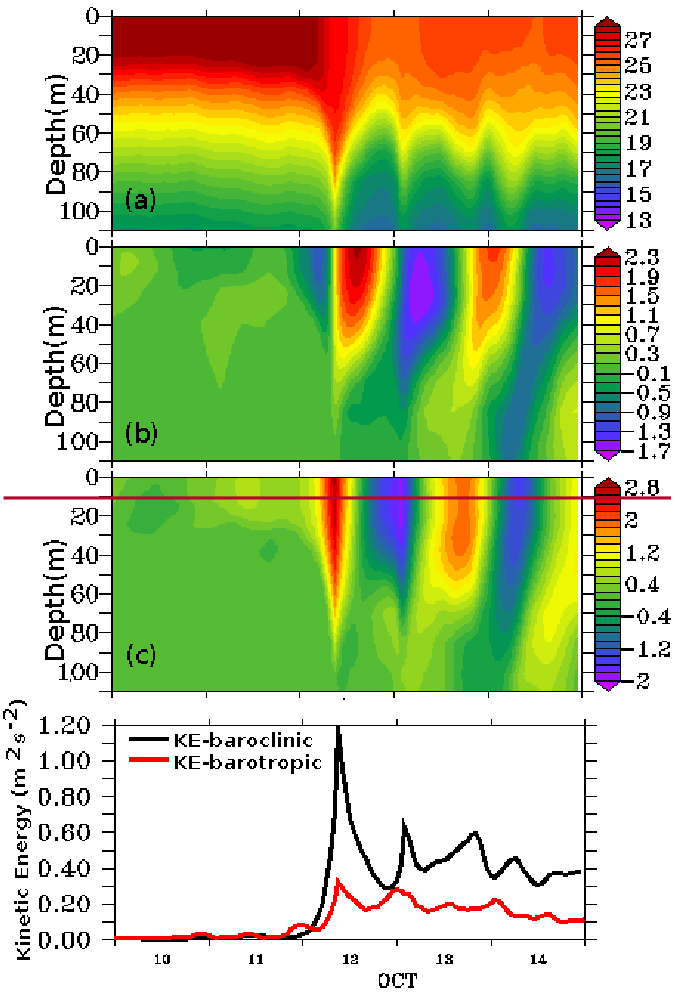
Depth(m)
0
20
40
60
80
100
(a)
27
25
23
21
19
17
15
13
(b)
2.3
1.9
1.5
1.1
0.7
0.3
-0.1
-0.5
-0.9
-1.3
-1.7
(c)
2.8
2
1.2
0.4
-0.4
-1.2
-2
Kinetic Energy (m 2 s -2)
1.20
1.00
0.80
0.60
0.40
0.20
0.00
KE-baroclinic
KE-barotropic
10
11
12
13
14
OCT

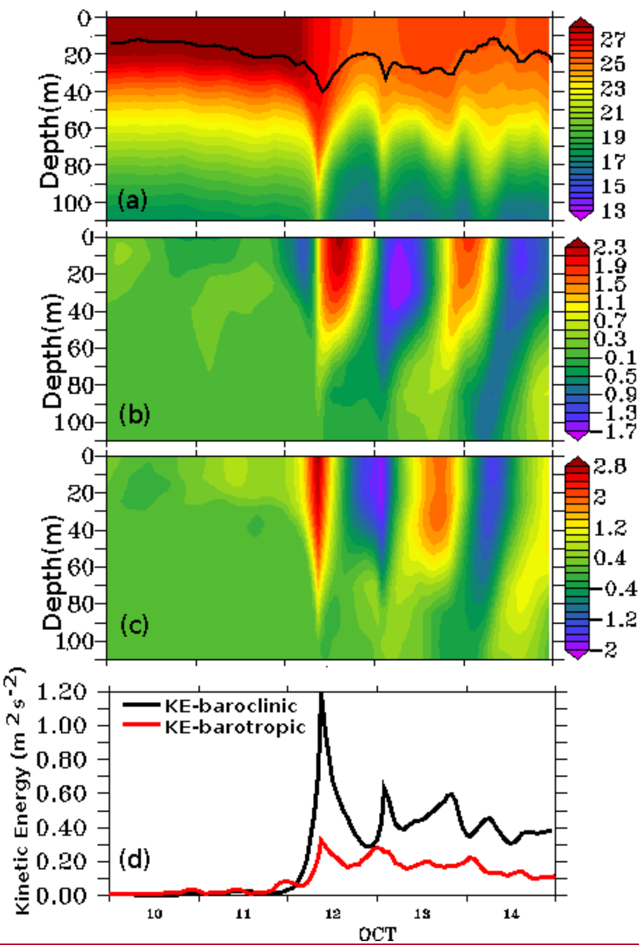

Figure 54:- The vertical profiles of temperature in °C (a), zonal current in m s^{-1} (b), meridional current in m s^{-1} (c). The kinetic energy (m^2s^{-2}) of baroclinic current (black) and barotropic current ($\times10^{-2}$) (red) (d). The thick black line in (a) denotes the mixed layer depth.

678 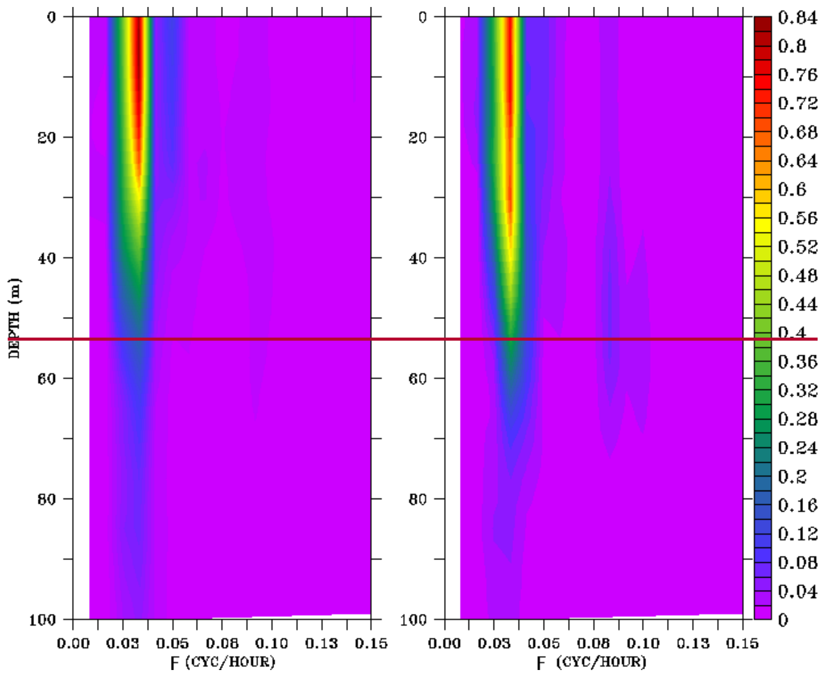

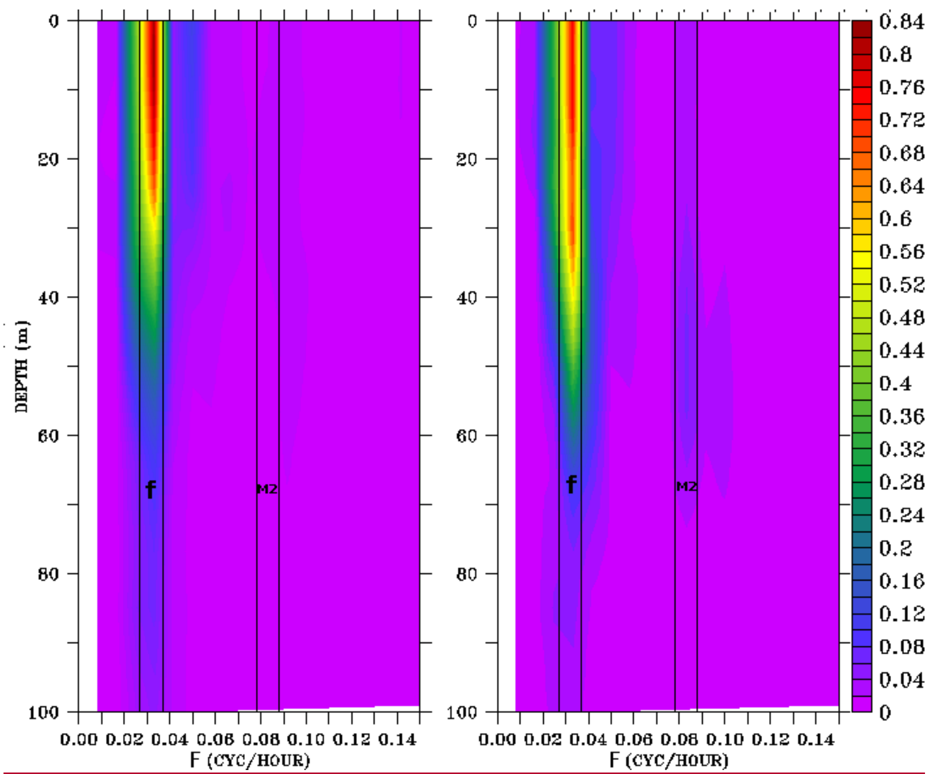

Figure 6~~5~~:- The power spectrum analysis (m^2s^{-1}) for a) baroclinic zonal current and b) baroclinic meridional current

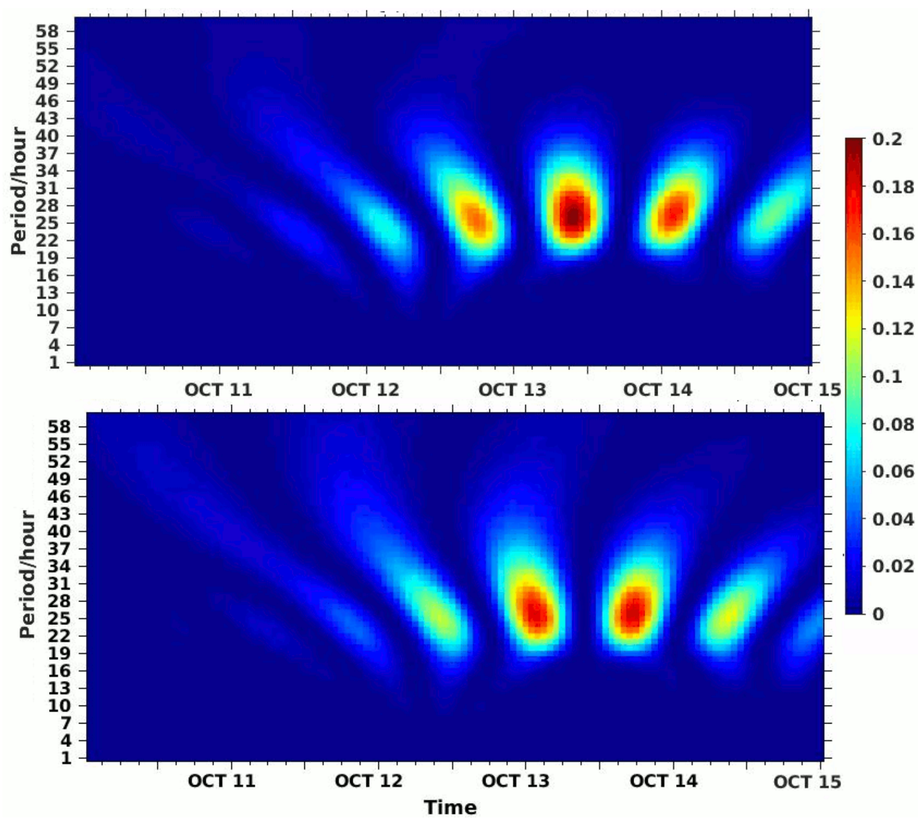

Figure 7~~6~~:- The scalogram in percentage at 40 m depth by continuous wavelet transform (CWT) method. Wavelet scalogram shown for the zonal baroclinic current (upper panel) and for the meridional baroclinic current (lower panel). ~~The white dashed line indicates the peak percentage of energy.~~

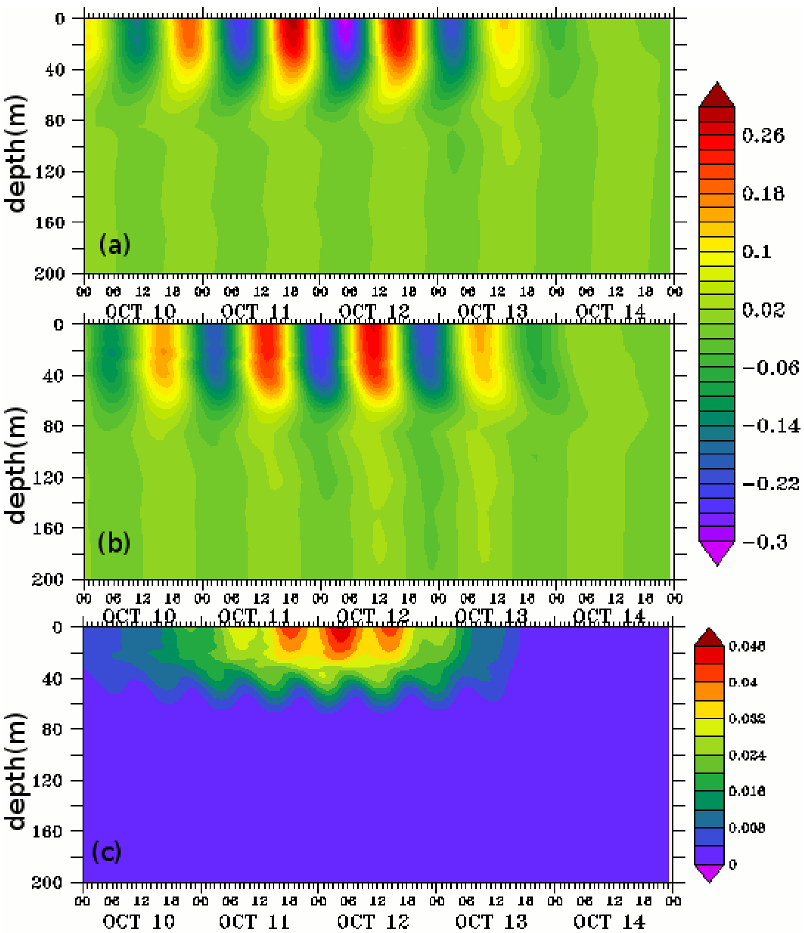

Figure 8~~7~~:- The profiles of a) near inertial zonal baroclinic current (U_f) b) near inertial meridional current (V_f) in m s^{-1} and c) Kinetic energy (E_f) of near inertial flow in m^2s^{-2}

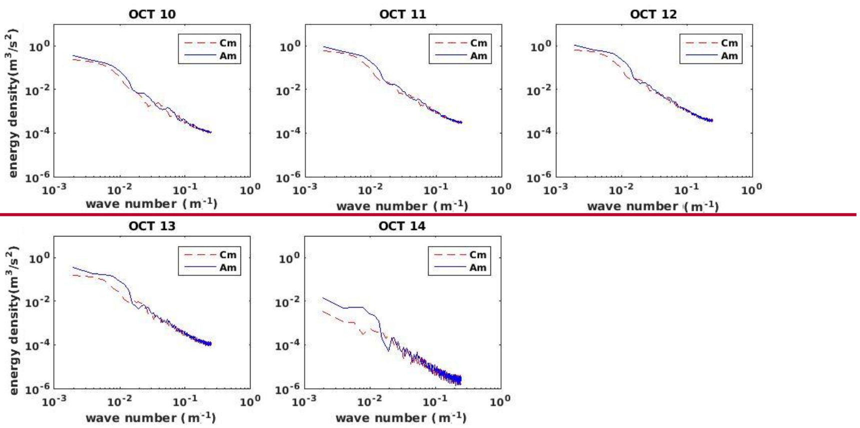

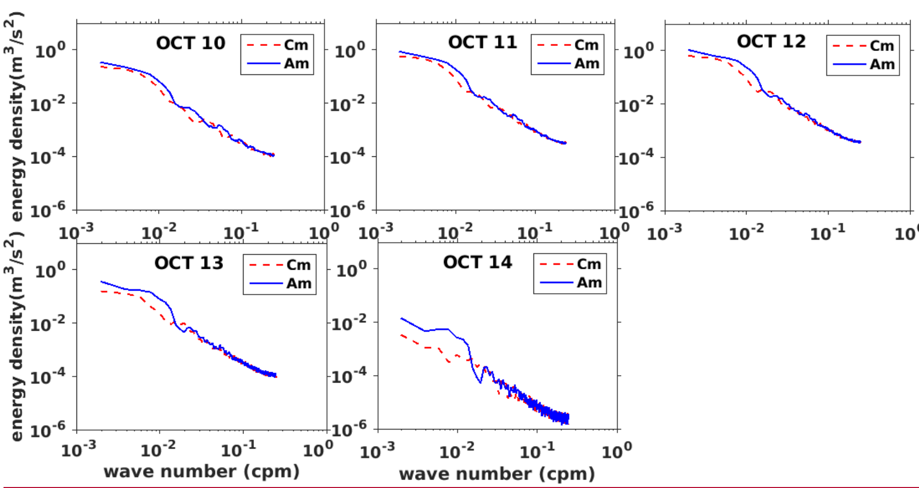

Figure 98:- The daily averaged vertical wave-number rotary spectra of near inertial oscillations. The anticyclonic and cyclonic spectra are represented in blue and dotted red lines respectively.

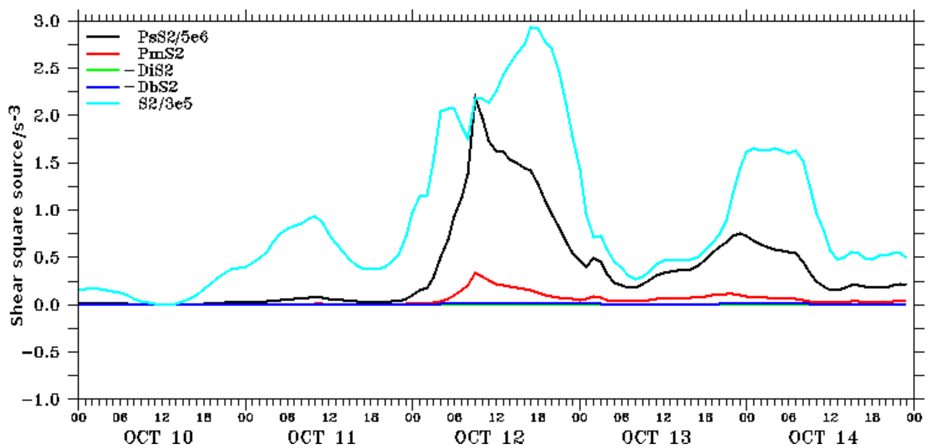

Figure 10~~9~~:- The model simulated bulk properties at the selected point location. The vertical shear square axis is multiplied with a factor of 10^{-6}. The magnitude of bulk shear squared S^2 (cyan color), surface wind stress P_sS^2 (black color), barotropic effect P_mS^2 (red color), bottom stress $-D_bS^2$ (blue color), interfacial friction $-D_iS^2$ (green color)

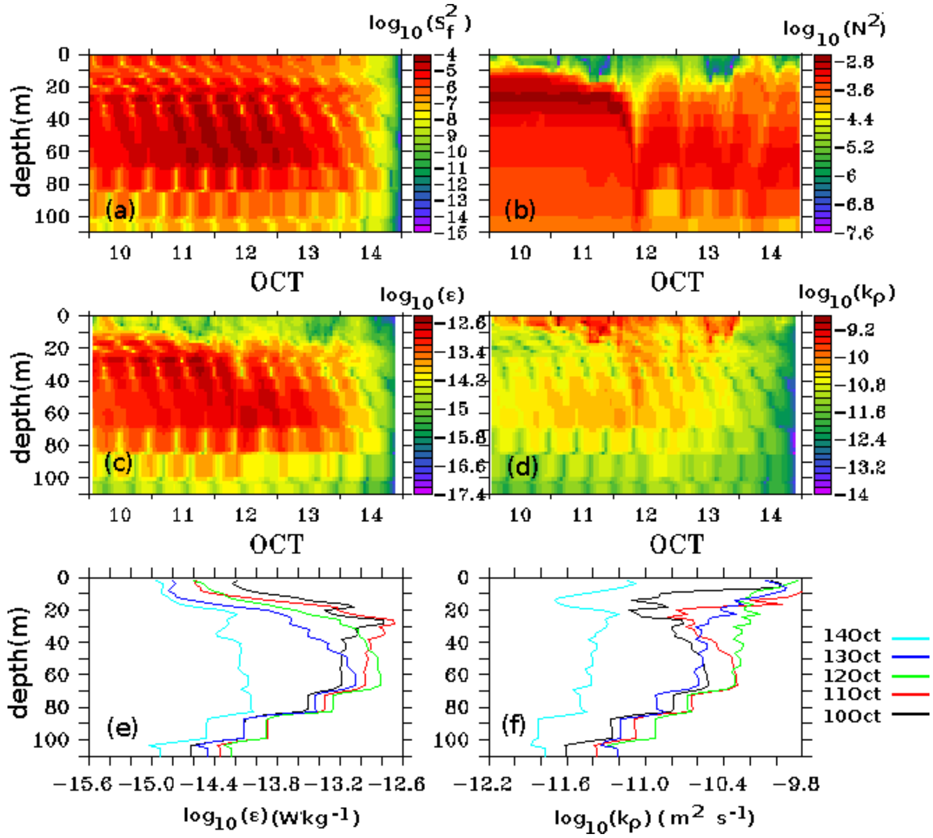

Figure 11~~10~~:- Profiles of a) velocity shear $\log_{10}(S^2)$, b) buoyancy frequency $\log_{10}(N^2)$, c) turbulent kinetic energy dissipation rate $\log_{10}(\varepsilon)$, d) turbulent eddy diffusivity $\log_{10}(K\rho)$, e) and f) are daily averaged turbulent kinetic energy dissipation rate and turbulent eddy diffusivity respectively